Journal of Nuclear Materials 448 (2014) 497–511

Contents lists available at ScienceDirect

Journal of Nuclear Materials

journal homepage: www.elsevier.com/locate/jnucmat

Radiation-tolerant joining technologies for silicon carbide ceramics and composites

Yutai Katoh [a,*], Lance L. Snead [a], Ting Cheng [a], Chunghao Shih [a], W. Daniel Lewis [a], Takaaki Koyanagi [b], Tatsuya Hinoki [b], Charles H. Henager Jr. [c], Monica Ferraris [d]

[a] Oak Ridge National Laboratory, P.O. Box 2008, Oak Ridge, Tennessee 37831, United States
[b] Institute of Advanced Energy, Kyoto University, Uji, Kyoto 611-0011, Japan
[c] Pacific Northwest National Laboratory, 902 Battelle Blvd., Richland, WA 99352, United States
[d] Department of Applied Science and Technology, Politecnico di Torino, Corso Duca degli Abruzzi 24, I-10129 Torino, Italy

ARTICLE INFO

Article history:
Available online 10 October 2013

ABSTRACT

Silicon carbide (SiC) for nuclear structural applications, whether in the monolithic ceramic or composite form, will require a robust joining technology capable of withstanding the harsh nuclear environment. This paper presents significant progress made towards identifying and processing irradiation-tolerant joining methods for nuclear-grade SiC. In doing so, a standardized methodology for carrying out joint testing has been established consistent with the small volume samples mandated by neutron irradiation testing. Candidate joining technologies were limited to those that provide low induced radioactivity and included titanium diffusion bonding, Ti–Si–C MAX-phase joining, calcia–alumina glass–ceramic joining, and transient eutectic-phase SiC joining. Samples of these joints were irradiated in the Oak Ridge National Laboratory High Flux Isotope Reactor at 500 or 800 °C, and their microstructure and mechanical properties were compared to pre-irradiation conditions. Within the limitations of statistics, all joining methodologies presented retained their joint mechanical strength to ~3 dpa at 500 °C, thus indicating the first results obtained on irradiation-stable SiC joints. Under the more aggressive irradiation conditions (800 °C, ~5 dpa), some joint materials exhibited significant irradiation-induced microstructural evolution; however, the effect of irradiation on joint strength appeared rather limited.

1. Introduction

The use of silicon carbide (SiC) composites in nuclear power applications, primarily fusion reactor structural elements or light-water reactor (LWR) fuel cladding and core constituents, has received increasing attention over the past decade and has been discussed as a critical need over the past two decades [1–3] for conceptual fusion reactor designs such as the European TAURO design [3], the US ARIES-AT and ARIES-ACT designs [4,5], and the Japanese DREAM [6]. Fig. 1 gives a schematic representation of the TAURO design, essentially consisting of nested plates made from SiC composite that form a simple compartmentalized box design in which the first wall and blanket internals are separately cooled by Pb-17Li. The ARIES-AT concept is of a similar design, again utilizing SiC composite and Pb-17Li coolant, in fairly simple geometry for ease of fabrication and joining. At the time of these fusion reactor designs, joining technologies were not specified.

For fission power applications, two generic design types employing SiC composites for LWR cladding are under discussion: fully ceramic SiC cladding and ceramic/metal cladding. For the fully ceramic cladding, some combination of fibrous composite is utilized to achieve fracture resistance and high-temperature performance with a single layer or multiple layers of monolithic SiC ceramic used to seal the inherently porous and microcracked composite. Using the metal/ceramic design, sealing is achieved either by an inner metallic bladder (liner) or outer metallic seal. For the fully ceramic system, an end-cap seal is required, which is a critical technology development still awaiting a solution.

As previously stated, the ability of joining SiC to itself or other materials is a critical, unresolved technological need regarding the application of SiC ceramics and composites in nuclear systems. This is in contrast to the ability to join SiC or SiC/SiC for non-nuclear applications, which can be accomplished in a reliable and rugged manner through a number of conventional and advanced techniques. The suite of nominally conventional techniques that has been successfully demonstrated includes pre-ceramic polymer joining, glass–ceramics, reaction bonding, active metal/pre-ceramic polymers, and active metal solid state displacement reactions. Additional details of these methods are provided in Section 2 of this paper. Although comparison of results from different studies on the strength of various bonding techniques is confounded by

* Corresponding author. Tel.: +1 865 576 5996; fax: +1 865 241 3650.
E-mail addresses: katohy@ornl.gov, katohy@gmail.com (Y. Katoh).

0022-3115/$ - see front matter © 2013 Elsevier B.V. All rights reserved.
http://dx.doi.org/10.1016/j.jnucmat.2013.10.002

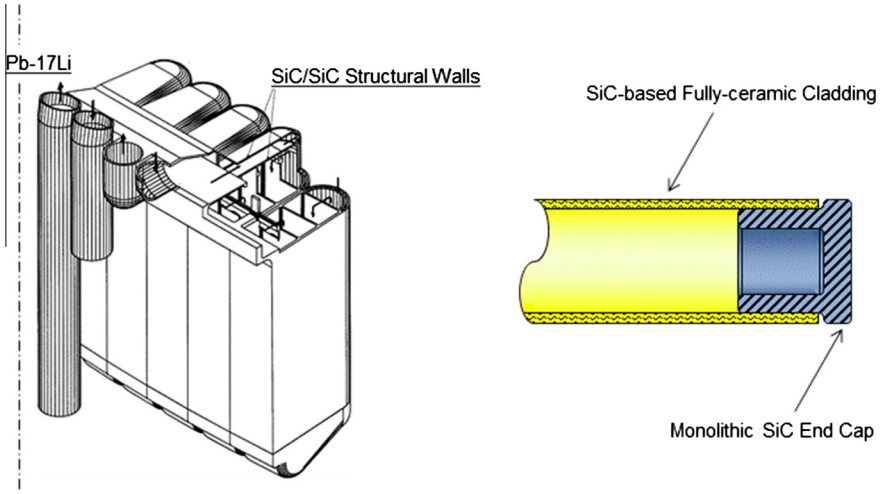

Fig. 1. Conceptual schematic of TAURO blanket design (left) and end plug section of fully ceramic LWR fuel rod (right).

a lack of standards for testing and the variety of test types used (e.g., bend vs tensile, etc.), the strength of the joints produced appears adequate for fusion and nuclear applications.

A key issue is that the methods studied to date, and the limited data available on the irradiation of joints and the materials making up those joints, have demonstrated poor irradiation stability. As discussed previously, a reliable joining technique for SiC still remains to be developed for nuclear applications. This is why mechanical component designs for near-term applications (such as control rod sleeves for high-temperature gas-cooled reactors) avoid the issue of joining entirely, preferring instead to use mechanical joints [7,8]. However, this option is not possible for fusion blanket systems, which require leak-tightness to PbLi or in some cases helium, or in the case of LWR cladding, as hermeticity (the retention of fission products and helium) is a functional requirement.

Another issue related to joining of SiC is the lack of a widely accepted standard test method: a reliable test not prohibitively difficult and/or expensive to prepare and capable of yielding reproducible shear strength is still unavailable [9]. An additional concern for nuclear applications is the use of miniaturized specimens necessary for testing irradiated samples. Torsion of solid specimens seems to be the appropriate test method for post-irradiation shear properties of joints of SiC-based materials [10]. The optimization of torsional specimen size and geometry was performed through the collaborative efforts of Oak Ridge National Laboratory (USA), Kyoto University (Japan), and Politecnico di Torino (Italy). Based on this development, a reliable comparison among different joints before and after neutron irradiation is presented in this work.

2. Joining technologies for silicon carbide

Various methods have either already been established or are currently considered promising for joining SiC to SiC, either monolithic or composite, for non-nuclear applications. These methods include solid state sintering of SiC ceramics, diffusion bonding using various active fillers [11], transient eutectic-phase routes [12–15], glass–ceramic joining [9,10,16], metallic braze-based joining [17–20], SiC reaction forming [21–23], MAX-phase bonding [24], pre-ceramic polymer routes [25–27], and selective area chemical vapor deposition (CVD) [28], to name a few. Joining processes that utilize solid state diffusion or transient liquid phases may often be assisted by additional local/internal heating schemes such as laser, electron beam, and pulsed electrical field (as used for spark plasma sintering) applications. When these techniques are discussed for application in nuclear environments, consideration must be given to issues related with neutron irradiation, in addition to those common to non-nuclear applications: strength and reliability during mechanical loading, required pressure for processing, potential process-induced damages to the base materials, chemical compatibility of the joint with the specific operating environment, and the ability to satisfy the design-specific hermeticity requirement. Specific to fusion applications is the strong bias towards materials with low induced radioactivity to ensure the structure remains a "low-activation" component. Below, representative joining methods for SiC ceramics and composites are briefly reviewed and discussed in terms of potential critical issues for applications in fusion and nuclear energy systems.

2.1. Solid state diffusion bonding

SiC to SiC can be achieved through a purely solid state self-diffusion process at very high temperatures and high pressure. This is obviously the ideal method, along with the selected area CVD, for producing a robust permanent joint in terms of chemical purity and structural continuity. However, considering that self-diffusion bonding typically requires high pressure at a temperature of at least $0.75T_m$, its utilization in practical applications will be severely limited, although the field-assisted technique achieves adequate bonding at a "low" temperature of ~2000 °C.

Far more common methods to join SiC to SiC are metal diffusion bonding techniques, which are accomplished by solid-state diffusive conversion of a metal insert into compounds with the host elements, silicide and/or carbide with SiC, to produce strong joints [29,30]. Metal diffusion bonding of SiC has been successfully achieved with various refractory metals, such as titanium, molybdenum, tantalum, niobium, and tungsten, which form carbides that are thermodynamically more stable than SiC [11]:

$$(xy)\mathrm{SiC} + (x+y)\mathrm{M} \rightarrow (y)\mathrm{MC}_x + (x)\mathrm{MSi}_y. \quad (1)$$

Solid state diffusion for these metals is generally fast enough at temperatures higher than ~1200 °C to result in full conversion of a thin metal foil (tens of microns) insert or powder slurry into the ceramic phases. Titanium makes Ti–Si–C ternary MAX phases in addition to the binary conversion products under certain conditions, and these are specifically classified as MAX-phase joining. The strength of the metal diffusion bonding is generally determined

by the fracture toughness of the conversion phases or the interfaces, volume change upon production of the carbide and/or silicide, and differences in the physical properties between the host ceramic and the conversion product phases.

Titanium is commonly used for the metal diffusion bonding of SiC. Titanium-joined SiC provides adequate strength, often exceeding 100 MPa in the shear mode, though this strength is often limited by a major mismatch in the coefficient of thermal expansion (CTE) between TiC and SiC. The process parameters, mainly temperature and hold time, determine the spatial and fractional distributions of the common reaction products among TiC, $Ti_5Si_3(C_x)$, and Ti_3SiC_2 [30]. Thus it is possible to minimize the CTE mismatch effect by process optimization.

Molybdenum diffusion bonding is reported to produce SiC joints with enhanced robustness [11], while tungsten may be the preferred joining agent for fusion from the standpoint of long-term activation. Cockeram reports qualitatively reasonable joining of CVD SiC through tungsten-insert solid state diffusion [31].

2.2. Transient eutectic-phase joining

Transient eutectic-phase (TEP) joining, often referred to as liquid-phase sintering (LPS) for ceramics processing, is a common technique used to produce silicide ceramics in monolith form. The TEP technique utilizes dissolution-reprecipitation processes of silicide ceramics with the silica-alumina-rare earth oxide eutectics to obtain a dense body [32]. The TEP process for producing SiC can be categorized as either pressureless or pressurized processes. Pressureless sintering is often adequate for low-cost production of SiC-dispersed ceramics, whereas pressurized sintering offers increased SiC volume fractions, leading to superior performance. The TEP processes are also used to join both metals and ceramics. For joining SiC, it is most straightforward to use a powder mixture, such as a SiC–alumina–yttria system, in which sintered SiC is the joining agent. Sintering the SiC base materials together using a SiC-free or silica-free joining agent is also an option [13]. A pressureless TEP process may be combined with the laser- or electron beam-assisted local heating to achieve pressureless joining [13].

A special category of pressurized TEP process named nano-infiltration and transient eutectic-phase (NITE) process was developed by Katoh et al., for production of SiC-matrix composites [33,34]. The NITE process, using nano-phase SiC powder precursor and limited quantity of sintering additives produces high quality SiC at a relatively low sintering temperature, which is suitable for joining SiC composites. NITE-like SiC-based joining was successfully accomplished, in which SiC joints of very high strength were demonstrated [12,15]. NITE-like joining may be performed either by applying the mixed powder in slurry or other forms or by using a commercial green sheet [15]. This joining process reportedly produces the best results when pressure in a typical range of 5–20 MPa is applied at a relatively high temperature of ~1800 °C. Since the NITE SiC/SiC composites and the monolithic NITE-like sintered SiC have demonstrated promising radiation resistance [35], the NITE joint is anticipated to also exhibit reasonable tolerance against neutron irradiation.

2.3. Glass–ceramic joining

Glass–ceramics joining, another promising method used to join ceramics in non-nuclear applications, is potentially useful for joining SiC ceramics and composites for fusion and nuclear energy applications because of (1) the relatively low temperature and low pressure required for joining, (2) the gas tightness and potential self-healing at high temperatures due to presence of a residual glassy phase, (3) the low activation properties for properly selected compositions, and (4) the ability to tailor CTE and microstructures. Development of glass–ceramic joining has been studied by Ferraris et al., who have produced promising joints of SiC composites using several systems including silica–alumina–yttria (SAY) [36] and calcia–alumina (CA) [10,37].

The use of glass–ceramics as joining materials in a high radiation environment is debatable. A few studies have been conducted on neutron irradiation of glass ceramics [38,39]. Two competing processes, swelling and densification of amorphous and crystalline phases present in a glass–ceramic, are known. It is also known and predictable that differential swelling/shrinking of the two phases can lead to a reduction in strength and ultimately to separation of the phases and eventual destruction of the material. However, recent results from neutron irradiation in High Flux Reactor (Petten) up to $\sim 3 \times 10^{25}$ n/m^2 ($E > 1$ MeV) at 600–820 °C showed only limited effects of irradiation on the phase stability, microstructure, and strength of the SAY glass–ceramic-joined SiC composite [36].

Moreover, a designed balance between swelling and shrinkage could lead to a glass–ceramic joining material that could be used in a pressureless joining method. Such feature could be of importance when large components have to be joined. A few glass–ceramics are currently under evaluation as pressureless joining materials for nuclear environment [9,10,16]. Common considerations associated with the use of glass–ceramics for nuclear applications are if extensive microcracking occurs due to differential swelling in a multi-phase joint and, similar to the reaction-bonded joint, if that microcracking can affect strength and permeability properties.

2.4. Metallic braze-based joining

A substantial amount of research and commercial development has been conducted on metallic braze-based joining technologies for SiC: the rationale behind it is the intrinsically safer mechanical behavior of a tough metallic joining material than that of brittle ceramic joints. Moreover, brazing technology that does not require pressure will be better suited to joining of large and/or complex components. Note that silver-based brazing technologies are not discussed in this paper due to the activation issue.

Originally developed by CEA in France for nuclear applications and commercialized by Snecma [19], the BraSiC™ formulation has found modest use in non-nuclear applications: several patents and a few technical papers describe this family of brazing alloys based on metal silicides [40–43]. These alloys are primarily M:Si alloys, where "M" represents metals of Cr, V, Ti, Rh, etc. Different BraSiC formulations are achieved by different M brazing atmospheres, resulting in a controlled and quite complete infiltration of the composite. Brazing is achieved using a pressureless process at temperatures ranging from 1200 to 1800 °C. Respectable shear strengths (80–100 MPa at 800 °C) have been reported. The main concern from a nuclear application standpoint is that the presence of residual silicon has been shown, in monolithic SiC, to reduce strength due to anisotropic swelling of the different phases [44–46].

Recently, an approach utilizing a multiphase braze alloy consisting of silicon and aluminum was developed by the Edison Welding Institute (Columbus, Ohio) [47]. The process results in a continuous primarily silicon braze joint containing discontinuous Al_4C_3 particles where aluminum comes into contact with SiC. Minor amounts of iron are also present. The process can be carried out at a low temperature (~1200 °C), and the samples did not fail during neutron irradiation in the Ohio State University research reactor to ~1 milli-dpa. While the resulting bonds are claimed to be strong, there remain concerns regarding their stability in a radiation or water environment. As discussed in Ref. [47], and confirmed

through the work of Corelli et al. [44], Matthews [45], and Matheny and Corelli [46], the differential dimensional stability of silicon and SiC results in stress-induced microcracking.

2.5. Si–C reaction bonding

Reaction forming of SiC, another technique to form SiC-based material to join SiC, is achieved most commonly by the direct reaction of silicon and carbon. The typical technical approach is to heat the pre-mixed joining formula to slightly above the melting point of silicon. During this process, the volume expansion upon conversion of carbon into SiC progressively microcracks the already formed SiC, letting capillary force drive molten silicon further into unreacted areas until the carbonaceous precursor is fully consumed. Therefore, the resultant joint microstructures consist of two distinct phases, namely, crystalline and stoichiometric SiC and the unreacted metallic silicon. The volume fraction of unreacted silicon may be reduced to ~10% when the process is optimized for reduced silicon content in the final product [48].

The direct Si–C reaction bonding has not been paid much attention for nuclear applications due to the well-known detrimental effect of the SiC–Si dual-phase microstructures on radiation stability, as mentioned above [44–46]. Matheny and Corelli reports the onset of substantial strength degradation of reaction-bonded SiC at a fluence between 2×10^{23} and 2×10^{24} n/m^2 ($E > 1$ MeV), presumably corresponding to ~0.03 and ~0.3 dpa, respectively, at an irradiation temperature of ~130 °C [46]. Although credible information about the swelling behavior of neutron-irradiated silicon is unavailable, it is reasonable to speculate that the typical cracking strain on order of ~0.1% for brittle ceramics is reached in this fluence range where SiC is anticipated to linearly swell by ~0.15% to ~1% at this temperature [49].

It is obvious that the differential swelling issue becomes critical when the volume fraction of the second phase is substantial, both phases are brittle, and there is no effective mechanism such as thermal or irradiation creep operating to mitigate the developing stress. This is likely the case for the reaction-bonded SiC. However, consequences of the differential swelling may be minimized when the microstructure is optimized so that the minimum amount of unreacted silicon is distributed as tiny grains within the continuum of the SiC matrix. Such microstructures have been demonstrated by Suyama et al. [48].

The reaction bonding can be applied in vacuum, inert, or oxidative atmospheres. While the capability of joining in air is a great benefit, when processed in air, silica is formed in the joint layer in addition to SiC and unreacted silicon found after joining in an inert atmosphere. As with the presence of silicon, silica has produced an unmatched dimensional change with irradiation (a contraction as compared to the swelling of SiC [50]) and would therefore be considered a concern as a bonding constituent.

2.6. MAX-phase joining

Some of the MAX-phase ceramics including Ti_3SiC_2 are known to offer high-temperature strength, pseudo-ductility or damage tolerance, and oxidation resistance [51]. The Ti_3SiC_2 MAX-phase joining of SiC and SiC-composite may be achieved through multiple routes. Solid state diffusion bonding of SiC using titanium insert results in formation of Ti_3SiC_2 phase under certain processing conditions [30]. A recent study at Oak Ridge National Laboratory (ORNL) confirmed that a near-single-phase Ti_3SiC_2 joint may be produced via this method [52]. Dong et al. reported successful joining of SiC by hot pressing using pre-synthesized Ti_3SiC_2 powder as the bonding compound [53].

Alternatively, bulk composite material consisting of SiC–Ti_3SiC_2 with small amounts of TiC determined by the phase equilibria conditions has been produced using the displacement reaction between Si and TiC [54]:

$$3TiC + 2Si \rightarrow Ti_3SiC_2 + SiC. \quad (2)$$

The joint composition can be adjusted using the TiC:Si ratio. [24,55–57]. When applied to joining SiC for nuclear applications, the joints are characterized by high strengths and low activation. Pacific Northwest National Laboratory (PNNL) has developed a tape casting process to join ceramics using this reaction. Henager and Kurtz report adequate strength and fracture toughness for the Hexoloy sintered SiC and Hi-Nicalon™ Type-S CVI SiC composite joints, prepared by the PNNL tape casting process, at temperatures up to ~1000 °C [55].

The Ti_3SiC_2 MAX-phase joining for SiC has not previously been evaluated for the effects of irradiation or optimized for irradiated properties. Limited publications on irradiation effects on the bulk Ti_3SiC_2 imply moderate radiation stability for ceramic materials based mainly on microstructural examination [58,59]. However, the effects of neutron irradiation on integrity are largely unknown for both bulk materials and joint structures.

2.7. Polymer-derived SiC joining

Preceramic polymers, such as polycarbosilanes and polysiloxanes, with inert and reactive fillers are used in SiC joining technologies [25–27,57,60,61] and have performed adequately as joints with moderate strength. Polycarbosilane, which converts to SiC, requires high-temperature processing and inert handling, while polysiloxanes, which convert to Si–O–C, can be pyrolyzed at lower temperatures and can be handled in air. Joints made from such materials exhibit strengths that range from 5 to 30 MPa when tested in shear. A known difficulty with preceramic polymers is mass loss, which can exceed 50%, on conversion to a ceramic phase. A slightly different approach uses a linear chain of polyhydridomethylsiloxane (PHMS) as a precursor to a highly crosslinked polysiloxane, by applying a catalytic chemistry approach developed at SRI International, that has the advantage of much lower mass loss on ceramic conversion compared to other systems, and pyrolysis occurs at temperatures as low as ~600 °C [24,62,63]. PHMS polymer converts to a silicon oxycarbide, which may be a disadvantage in terms of creep strength and corrosion resistance depending on the structure and amount of free carbon [64].

Polymer-derived SiC products are in general unstable in a radiation environment, as well demonstrated by the neutron irradiation response of the ceramic-grade Nicalon™ fibers that are derived from polycarbosilane [65]. This is due to the intrinsic radiation instability of silicon oxycarbide and the nano-crystalline SiC-based structures. Certain polymers that convert to near-stoichiometric SiC [66,67] have the potential to produce radiation-stable SiC-based joints when combined with a crystallization treatment. However, achieving adequate mechanical properties for polymer-derived SiC after being fully crystallized is expected to be a challenge [68].

2.8. Summary of joining methods

Methods discussed in this section for joining SiC ceramics and composites are summarized in Table 1, along with typical reported strength properties and anticipated irradiation performance issues based on the chemistry and the microstructural information.

Table 1
Methods of joining SiC-based materials.

Method	Process condition	Material/phase in joint	Typical strength	Irradiation performance	Refs.
Solid state diffusion bonding	1200–1500 °C, 3–50 MPa	Ti_3SiC_2, $Ti_5Si_3C_x$, TiC, $TiSi_2$	Up to ~150 MPa shear	This work	[29,31,69]
	1500 °C, 3–17 MPa	$Mo_5Si_3C_x$, Mo_2C, what phase	~150 MPa DNS[1] shear	Unknown	[11]
	1500 °C, ~17 MPa	WC, W_2C, W_5Si_3	Not reported	Unknown	[31]
Transient eutectic-phase joining	1500–1900 °C, 5–20 MPa	SiC, Al–Y–O	Up to ~300 MPa tensile	Expectedly good	[15]
Glass–ceramic joining	1375 °C, pressureless	Mullite, cristobalite, keivyite	~100 MPa 4PB[2]	No degradation at a few dpa reported	[37]
	1480 °C, pressureless	$CaO–Al_2O_3$	~100 MPa torsional shear	This work	[10,37]
Metallic braze-based joining	~1400 °C, pressureless	Si, MSi_2 (M = Ti, Cr)	~100 MPa 4 PB or shear	Unknown	[70–72]
	~1000 °C, pressureless	Si, Al_4C_3	Not reported	No degradation at milli-dpa reported	[47]
Si–C reaction bonding	~1425 °C, pressureless	SiC, Si	Up to ~250 MPa 4 PB	Unknown	[18,21]
MAX-phase joining	~1450 °C, 30–40 MPa	Ti_3SiC_2, SiC	~400 MPa 4 PB	This work	[55]
Polymer-derived SiC joining	1000–1400 °C, pressureless	Si–O–C (–N)	Up to tens MPa, SLO[3] shear	Expectedly unstable	[57,73]
Selective area CVD	1000–1500 °C, pressureless	SiC	Not reported	Expectedly stable	[28]

[1] Double-notch shear.
[2] Four-point bending.
[3] Single-lap offset shear.

3. Experimental methods

3.1. Preparation of joint specimens

For the present irradiation effects study, the test specimens were prepared using diffusion bonding with the active titanium insert, TEP joining with NITE-like SiC, calcia–alumina (CA) glass–ceramics, and reaction-formed MAX-phase bonding, as summarized in Table 2. The designator column indicates the method of joining and the joined base material. For example, Ti/CVD denotes a joint of CVD SiC to CVD SiC prepared by the titanium diffusion bonding technique.

3.1.1. Titanium diffusion-bonded CVD SiC

A pure titanium foil (20 μm thick) was used for diffusion bonding of CVD SiC. The titanium foil was inserted between two plates of CVD SiC, and then a joint was formed by hot-pressing at 1443 K, held for 3 h, in an argon atmosphere, at a pressure of 20 MPa.

3.1.2. TEP-joined SiC ceramics and composite

Two types of NITE-like TEP joining were prepared in this work: the joining using mixed powder slurry (TEPs) and the joining with a commercial green tape (TEPt) both based on the NITE formula.

TEPs joining was adopted for CVD SiC and sintered monolithic SiC using the NITE formula (NITE-like sintered SiC; NLS SiC hereafter), and NITE SiC/SiC composite (pilot grade #3). The NITE slurry consists of SiC nano-phase powder (average diameters ~30 nm), and Al_2O_3 powder, Y_2O_3 powder, and SiO_2 powder. The total amount of oxide additives was 6 wt%. For the fabrication of NLS SiC, NITE slurry was sintered by hot-pressing at 1900 °C, for 1 h, in an Ar atmosphere, under a pressure of 20 MPa. To form TEPs joint, base materials sandwiching thin NITE slurry were hot-pressed. The conditions of the hot-pressing were identical with those for fabrication of NLS SiC.

TEPt joining was adopted for CVD SiC and NLS SiC. The green tape used (approximately 500 μm thick), consisting of SiC nano-phase powder and the Al_2O_3/Y_2O_3 sintering additives, was provided by IEST Co., Ltd., Japan. The TEPt joining was performed by hot-pressing at 1850 °C for 1 h in an Ar atmosphere under a pressure of 10 MPa.

3.1.3. CA glass–ceramic-joined CVD SiC

The CA glass–ceramic joint was prepared using $CaO–Al_2O_3$ (49.7 CaO, 50.3 Al_2O_3 wt%) glass. The joining material was designed, prepared, and characterized as described in Refs. [10,16,74]. The CA was synthesized by melt/quenching: the powdered raw products were melted in a platinum–rhodium crucible in air at 1750 °C for 30 min, and the glass then was poured on a brass plate and subsequently powdered and sieved. The joint samples were prepared by a pressureless slurry-based method: depositing CA slurry at room temperature on the surface of the pre-machined pieces of CVD SiC. The slurry is a mixture of as-cast CA powder (grain size 38–75 μm) dispersed in ethanol. A pair of half hourglass SiC parts were pressurelessly held together in a graphite holder with the CA slurry in-between, and then heated in a tubular oven under an argon flow for 10 min at 1480 °C.

3.1.4. Ti–Si–C MAX-phase-joined CVD SiC

The Ti–Si–C MAX-phase joint was prepared by a tape calendering process using organic binders and plasticizers together with a mixture of TiC and silicon powders, with 99.99% purity, average diameters less than 45 μm, and a TiC:Si ratio of 3:2. The flexible

Table 2
Joint materials prepared for this study.

Designator	Method of joining	Base material joined	Phases present in joint layer
Ti/CVD	Ti diffusion bonding	CVD SiC[1]	Ti_3SiC_2, Ti_5Si_3
TEPs/CVD	TEP/NITE SiC slurry	CVD SiC	SiC, YAG, Al_2O_3
TEPs/NLS		NITE-like sintered SiC[2]	
TEPs/NITE		NITE SiC/SiC[3]	
TEPt/CVD	TEP/NITE SiC tape	CVD SiC	SiC, YAG, Al_2O_3
TEPt/NLS		NITE-like sintered SiC	
CA/CVD	CA glass ceramic	CVD SiC	$12CaO·7Al_2O_3$, $3CaO·Al_2O_3$
TiSiC/CVD	Ti–Si–C MAX-phase	CVD SiC	Ti_3SiC_2, SiC

[1] Rohm and Haas CVD SiC.
[2] Matrix material for NITE SiC/SiC composite.
[3] Cross-ply architecture.

calendered tapes were 200 μm thick and were cut to shape and applied between two pre-machined CVD SiC coupons. Joints were formed by heating the coupon sandwiches in argon to 1425 °C at 10 K/min and holding for 2 h at 30–40 MPa applied pressure. The extensive research conducted at PNNL has demonstrated that at least 30 MPa of applied pressure during joining is required for full joint density. The resulting joints were approximately 12–30 μm thick [24,55].

It should be noted that the specimens of the titanium diffusion-bonded and TEP joined materials were machined after lap-joining of a pair of flat plates of the base material was completed, whereas the specimens of the CA glass–ceramic and the MAX-phase joints were individually prepared by joining a pair of pre-machined half specimens in alignment fixture. The effect of processing/machining time order on the strength of the joint specimens may not be significant.

3.2. Strength evaluation

One of the challenges facing ceramic joint development efforts is the lack of adequate standardized testing methods to ensure the acquisition of mechanical properties data in a reliable and reproducible manner. This is particularly the case when limitations are imposed on specimen geometry/dimensions or when complex test procedures are required because of limited flexibility in irradiation experiments. The failure modes of primary interest in ceramic joints are shear and tension. Of these, shear is the more common mode of failure. Simple methods such as single lap offset shear, double-notched shear, and asymmetric four point bending are frequently adopted for shear strength determination of ceramic composite joints [24,75]. However, as shown in Table 3, which lists the methods applicable for shear or apparent shear properties evaluation of ceramic composite joints, only the torsional configuration is capable of producing true shear loading and appropriate for testing lap-joined small specimens. Moreover, a systematic study conducted in support of this work indicated that the apparent strength values determined by the single lap offset shear test often significantly deviate from the results of tests in a true shear loading state [24,75]. For these reasons, torsional testing was chosen as the method for determining joint shear strength in this study, even though evaluation of the ability of this test to determine true shear strength has not yet been completed. Details of torsional shear test development are reported by Ferraris et al. [37] and Jung et al. [76].

The torsional shear specimen types 6SQ-5D and -4D were specifically chosen for this neutron irradiation study. As shown in Fig. 2, these specimens have the envelope dimensions of 6 mm × 6 mm × 3 mm, allowing them to fit in the small interior of an irradiation capsules and to minimize the radiological concerns during post-irradiation evaluation. The potential drawbacks and issues associated with these miniature specimens having very short fillet section length and the square grip sections include the non-linear stress distribution within the joint layer with regard to the distance from torsional axis, a slight periodic variation of stress magnitude along the circumference due to the grip shape, and the resultant non-explicit correlation between the true and the analytical maximum shear stresses. However, the nominal shear strength values (τ_{th}) reported in the paper are given by

$$\tau_{th} = 16T/\pi d^3, \quad (3)$$

where T is the applied torque and d is the specimen (fillet) diameter at the joint plane. Note that the shear strength values measured in this work would be better defined as the torsion resistance of these joined structures, and they can be safely used to compare torsional failure resistance of SiC hourglasses joined by several different materials. However, the term shear strength will be used instead of torsion resistance of joined structure for brevity.

3.3. Neutron irradiation

A series of irradiation experiments was carried out in the target irradiation facility of the HFIR using the rabbit irradiation vehicles. Sixteen test specimens of Type 6SQ-4D/5D miniature solid hourglass ceramic joints, typically four replicate specimens each for four material variations, were placed in a single rabbit capsule. Irradiation was carried out to approximately 3.0–3.4 × 10^{25} n/m^2 ($E > 0.1$ MeV) at 500 °C and 5.0 × 10^{25} n/m^2 ($E > 0.1$ MeV) at 800 °C. An equivalence of 1 × 10^{25} n/m^2 ($E > 0.1$ MeV) with 1 dpa in SiC is assumed in the following discussion. Of significance is that at this temperature range, which is within the transient swelling temperature regime for SiC, these fluences exceeded the saturation fluence such that no progressive dimensional change was anticipated for SiC with further irradiation [77]. Therefore, although the fluences were not high enough to fully address the radiation effect issues for fusion and nuclear applications, potential issues associated with the swelling of SiC should for the most part be revealed at these fluences.

3.4. Post-irradiation examination

Post-irradiation examination was carried out in the Low Activation Materials Development and Analysis (LAMDA) laboratory at ORNL. Detailed examination in LAMDA included torsional shear strength, fracture surface examination, and cross-sectional microstructures and micro-chemical analyses on a limited number of specimens. Details of the shear strength test procedure are given elsewhere [76]. Scanning electron microscopy (SEM) examination and analyses were performed using field-emission-gun SEM Hitachi Models S4700 and S4800, equipped with energy dispersive X-ray spectroscopy (EDS). The X-ray diffraction (XRD) analysis was performed using Thermo ARL Model Scinatag Pad V.

4. Results and discussion

4.1. Shear strengths

The joint processing conditions described earlier and the testing results are summarized in Table 4. Four replicate samples of each material were irradiated under different conditions such that a somewhat statistical comparison of unirradiated and irradiated samples could be made. The average shear strength and the range of scatter for each joint tested are graphically compared in Fig. 3. Shear strength in an unirradiated condition, as determined by the solid hourglass torsion test, in general appeared to be slightly over 100 MPa for titanium diffusion, CA, and Ti–Si–C bonded CVD SiC, whereas a shear strength of ~150 MPa or higher was obtained for all the TEP-bonded materials.

Shown together with the shear strength in Table 4 are the locations of the final fracture, as determined by visual inspection of the failed specimens. Failure at a joint denotes a flat debond entirely at the joint plane. In this type of failure, the roughness of the fracture surface does not exceed the thickness of the bonding layer. This failure occurs when the entire crack initiation and propagation processes take place along the bonding layer–substrate interface or within the bonding layer, suggesting a significantly lower fracture toughness of the joining material or the interface than that of the base material. An example of this type of fracture surface is shown in a three-dimensional digital micrograph in Fig. 4(A). In contrast, some fracture surfaces appeared entirely to be a bulk failure in the base material, as shown by Fig. 4(C). This type of

Table 3
Methods of shear (and apparent shear) properties evaluation available for ceramic joints.

Test method	Specimen geometry	Test requirement	Stress state	Example of test standard
Short beam flexure	Lap-joined beam	Adequate modulus-to-strength ratio	Mixed	ASTM D2344 (for FRP)
Single lap offset	Offset lap-joined coupon		Mixed; sharp stress concentration	ASTM D905
Double lap offset	Offset double-lap-joined coupon		Mixed; sharp stress concentration	
Double-notch shear	Lap-joined double-notched coupon		Mixed; sharp stress concentration	ASTM D3846 (for FRP)
Slant shear	Slant-butt-joined beam/coupon		Mixed	ASTM D3518 (for PMC)
Rail shear	Lap-joined coupon	Rigid mount on fixture	Mixed	ASTM D4255 (for FRP)
Torsion of solid rod	Lap- or butt-joined rod/hourglass	Torsion grip mechanism	Shear; non-uniform	ASTM F1362
Torsion of tube	Butt-joined hollow rod/hourglass	Torsion grip mechanism	Shear	ASTM D5448 (for PMC)
Asymmetric four point	Butt-joined beam	Strong base material	Shear	ASTM C1469
Iosipescu shear	Butt-joined notched beam		Shear	ASTM D5379 (for FRP)

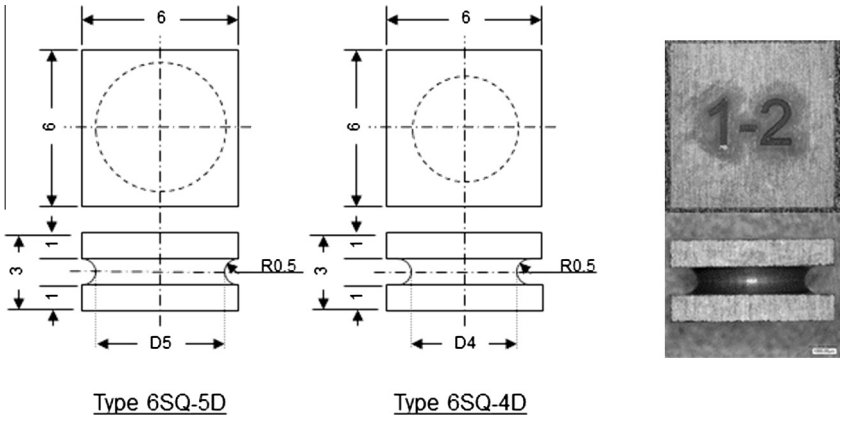

Fig. 2. Miniature hourglass test specimens used in the present study.

Table 4
Shear strength test results summary for SiC joints.

Joint	Strength, unirradiated (MPa)	Failure location, unirradiated	Irradiation condition	Strength, irradiated (MPa)	Failure location, irradiated
Ti/CVD	124 (23)[1]	J[2], P[3]	500 °C, 3.4 dpa	125 (36)	J, P
TEPs/CVD	150 (64)	B[4]	500 °C, 3.0–3.4 dpa	251 (40)	B
TEPs/NLS	335 (16)	B	500 °C, 3.4 dpa	349 (38)	B
TEPs/NITE	209 (14)	B	500 °C, 3.4 dpa	182 (21)	B
TEPt/CVD	150 (16)	B	500 °C, 3.0 dpa	139 (20)	B
			800 °C, 5.0 dpa	133 (13)	B
TEPt/NLS	172 (4)	B	500 °C, 3.0 dpa	126 (16)	B
			800 °C, 5.0 dpa	143 (10)	B
CA/CVD	115 (20)	J, P	500 °C, 3.0 dpa	93 (5)	J, P
			800 °C, 5.0 dpa	93 (6)	J
TiSiC/CVD	117 (10)	B	800 °C, 5.0 dpa	98 (22)	J

[1] Numbers in parentheses denote 1 standard deviation.
[2] Flat failure at joint plane.
[3] Failure partially at joint plane.
[4] Failure mostly in base material.

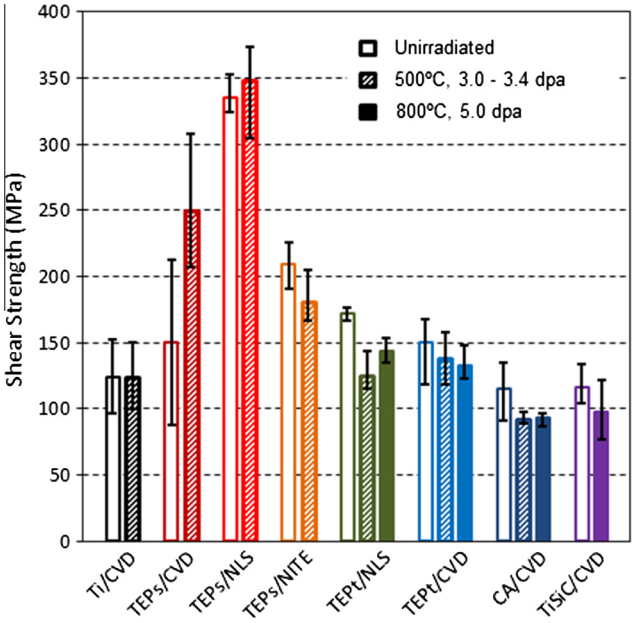

Fig. 3. Shear strength of multiple joints before and after neutron radiation. (Each error bar represents the maximum and minimum strength values for the joint.).

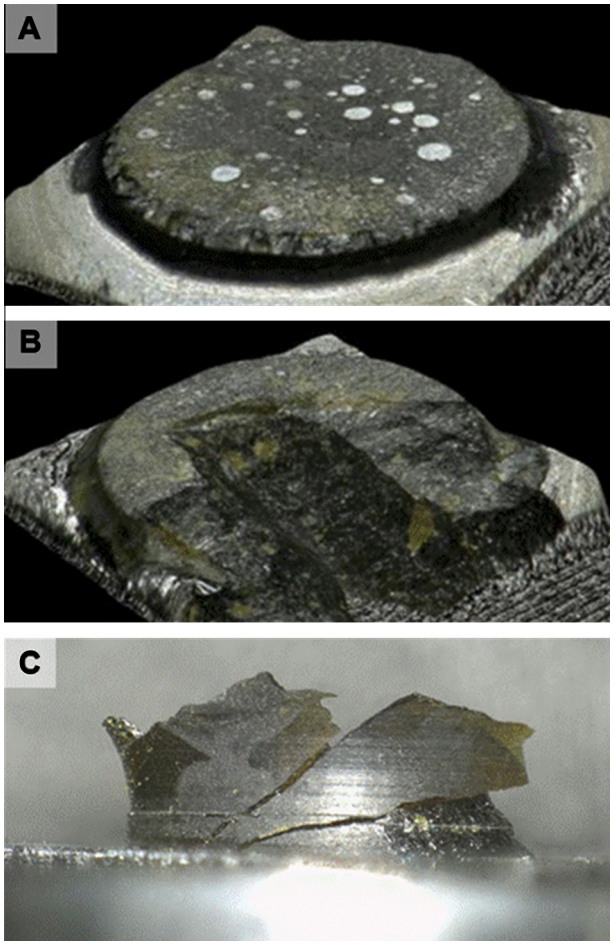

Fig. 4. Examples of fracture surfaces or cracking behaviors corresponding to flat failure at joint (A), partially flat failure at joint (B), and failure in base material (C). Note that cracks are deflected along the joint line to limited extents in example (C), which is not always the case for failure in base materials. Specimen diameter at the joint layer is 5 mm.

fracture often results in a shattering of the test specimen into small pieces upon an abrupt release of energy due to the high joint strength, making examination of the fracture surface challenging. In such cases, it is extremely difficult to identify the location of fracture origin, whether it was at the bonding or within the base material, upon examination of the fractured specimens. Joints of intermediate strength tend to exhibit the mixed fracture (partial failure at joint plane) shown in Fig. 4(B). It should be noted that factors other than the bonding strength, such as residual stress and difference in elastic modulus, may also influence the failure type.

After neutron irradiation to 3.0–3.4 dpa at 500 °C, the Ti/CVD joint showed a shear strength equivalent to that of the unirradiated specimen, indicating that neutron irradiation had not affected its strength under these conditions. This joint failed at the joint plane either entirely or partially in both the unirradiated and irradiated conditions. The CA/CVD joint retained ~81% of its unirradiated strength after neutron irradiation to 3 dpa at 500 °C and to 5 dpa at 800 °C. It was not possible to determine whether the observed changes were statistically significant due to the small specimen populations. However, while only one-half of CA/CVD specimens failed entirely at the joint plane before irradiation, all the specimens did so after irradiation at 800 °C. Similarly, the TiSiC/CVD retained ~84% of its unirradiated strength after neutron irradiation to 5 dpa at 800 °C, with a change in failure type from entirely base material failure to flat failure at the joint plane. While these slight changes in the average strength and transitions in the failure type imply the finite effects of irradiation on mechanical properties, no decisive conclusions may be drawn due to the limited specimen populations tested, as compared to the required statistics. Moreover, neutron irradiation reportedly increases the toughness of CVD SiC [77,78], and thus may contribute to altering the crack deflection criteria at the interfaces.

All the TEP joint specimens apparently failed in the base materials, regardless of the choice of base material, joining method between slurry and green tape, or irradiation condition. The failure observed in the base material denotes that the crack was not deflected within the bonding layer or at the bonding interfaces. Shear strength was not significantly decreased by neutron irradiation in any of the TEP joints, while it apparently increased in some cases. This observation indicates that the TEP joint itself did not degrade in strength, if at all, to an extent that would enable crack propagation within the bonded material or along its interface with the base material. The strength of NITE-like monolithic SiC reportedly decreased ~34% after neutron irradiation to 5.9 dpa at 830 °C [35]. This reported significant strength degradation may be attributed to the larger amount of sintering additives used for producing the test specimens in that work, 12 wt% as compared to 6 wt% in the present work.

However, the very significant increase in apparent shear strength for the TEPs/CVD after irradiation is considered an artifact: out of four specimens tested under unirradiated conditions, two specimens failed at ~100 MPa and the other two specimens failed at ~200 MPa. It is speculated that the weaker specimens failed due to non-uniform quality of the TEPs/CVD joints, whereas the stronger specimens likely represented the true torsion resistance of this joint.

4.2. Microstructures

4.2.1. Titanium diffusion-bonded CVD SiC

Backscattered electron images of the polished cross sections of the titanium diffusion-bonded CVD SiC specimens are shown in Fig. 5 before and after neutron irradiation to 3.4 dpa at 500 °C.

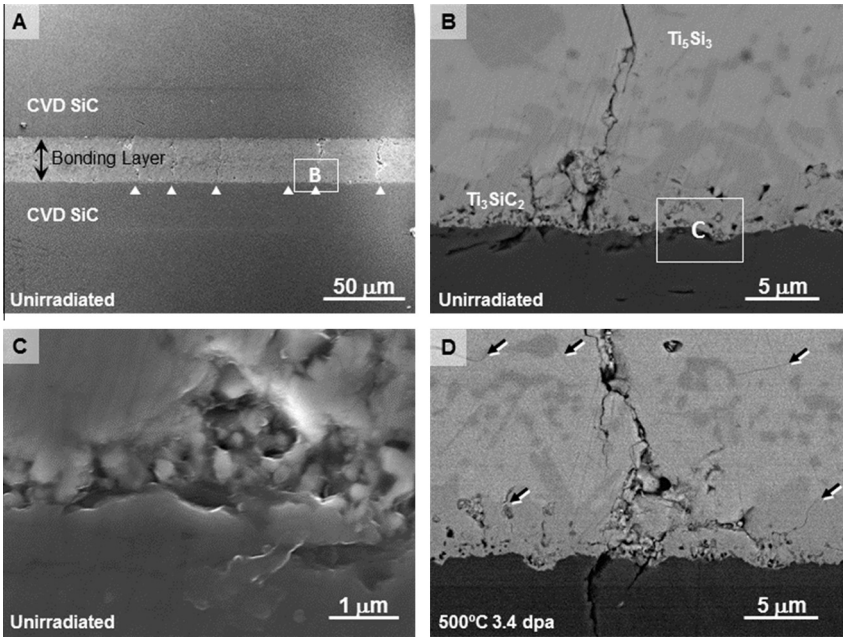

Fig. 5. Cross-sectional backscattered electron images of titanium diffusion-bonded CVD SiC in as-joined (A–C) and neutron-irradiated (D, 3.4 dpa at 500 °C) conditions. Triangular symbols in micrograph (A) indicate locations of the obvious transverse cracks. Arrows in subset (D) show microcracks. Micrographs B and C were taken approximately from locations shown by rectangles in micrographs A and B, respectively.

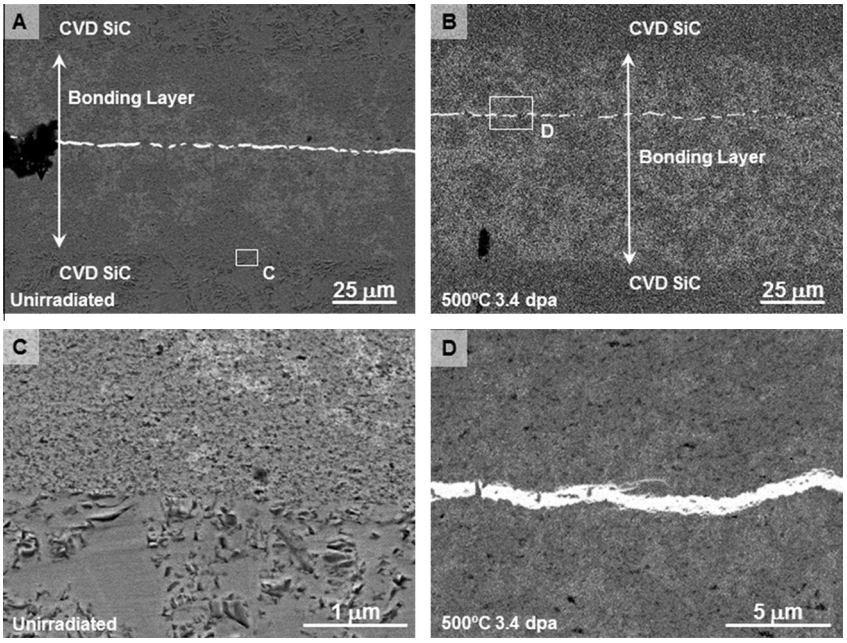

Fig. 6. Cross-sectional backscattered electron images of TEP (slurry) SiC-bonded CVD SiC in as-joined (A and C) and neutron-irradiated (B and D, 3.4 dpa at 500 °C) conditions. Micrographs C and D were taken approximately from locations shown by rectangles in micrographs A and B, respectively.

The as-joined microstructure indicates a complete conversion of the metallic titanium filler into a compound layer that consists of two distinct phases. The bonding layer thickness appeared to be ~27 μm as compared to the original titanium foil insert thickness of 20 μm. The XRD analysis indicated the presence of Ti_5Si_3 and Ti_3SiC_2 within the bonding layer. From the backscattered electron images, the phase interfacing with the base SiC is identified to be Ti_3SiC_2 and the phase dominating in near the mid-plane is identified to be Ti_5Si_3. This observation is consistent with the schematic structure reported by Gottselig et al. [30], except that no TiC phase was identified in the current study.

The bonding layer in the as-joined sample obviously contained defects. Major cracks were running across the bonding layer at an average spacing on order of 40–50 μm. Most of these cracks terminated at the interface with the base CVD SiC; however, some of them appeared to have propagated into the SiC. The driving force of this transverse cracking is understood to be the thermal stress resulting from a mismatch in thermal expansion during cooling from the processing temperature. The coefficient of thermal expansion (CTE) is reported to be ~5.9 and ~16.9 × 10^{-6} K^{-1} (RT to 1000 °C) for Ti_5Si_3 (*a*-axis and *c*-axis, respectively) [79] and ~8.6 and ~9.75 × 10^{-6} K^{-1} (RT to 1400 °C) for Ti_3SiC_2 (*a*-axis and *c*-axis,

respectively) [80], in contrast to a low value of $\sim 4 \times 10^{-6}\,K^{-1}$ (RT to 1000 °C) for SiC. The differences in CTE to these extents reasonably explain the extensive transverse cracking within the titanium compound layer. Because of these major transverse cracks at a high density, gas tightness may not be expected in this joint.

Another feature apparent from the micrographs is the porosity in the Ti_3SiC_2 along the interface with SiC, as highlighted in Fig. 5(C). It is possible for TiC to have formed along the interface, although it was not detected by XRD. However, because no deflection of the transverse cracks along the interfaces was observed, potential contribution from these micro-pores or possible TiC formation to the interface mechanical property is probably limited.

The post-irradiation specimen did not exhibit obvious changes in the main microstructural features discussed above, that is, the bi-phase bonding layer structure, the transverse cracks, and the slightly porous interface. However, though quantitative information was not obtained in the present work, the width of the transverse cracks seemed to have increased slightly after irradiation. Crystalline SiC is known to undergo swelling of slightly greater than 1% during irradiation at 500 °C and saturated by the dose in this experiment [77]. The swelling behavior of several other ceramics have been studied and known to vary [81–84]; however, no irradiation-induced swelling data are available for Ti_5Si_3 and Ti_3SiC_2. In case these titanium compounds undergo less swelling than SiC, the excess swelling of SiC should cause the crack opening in the bonding layer to increase. In addition, microcracks were present in both Ti_3SiC_2 and Ti_5Si_3 phases following irradiation, as shown in Fig. 5(D). This microcracking may be attributed to the irradiation-induced anisotropic deformation of hexagonal ceramics [85]. However, the joint strength remained almost unchanged because of the extensive transverse cracks that were already present before irradiation.

4.2.2. TEP slurry-joined CVD SiC and NITE-like SiC

Cross-sectional scanning electron images of the TEPs/CVD samples are shown in Fig. 6. No difference was apparent in the SEM microstructures between the TEPs/CVD and the TEPs/NLS joints except the NLS substrate involved scattered oxide and slightly higher porosity, both typical in the NITE-sintered SiC. The bonding layer, while not remarkably distinguishable from the CVD or NLS SiC substrates due to the stoichiometric SiC-based composition for the resultant sintered body, measured ~80 μm in thickness. This particular NITE-like TEP process is known to produce fully crystallized polycrystalline SiC with sub-micron grains of primarily beta-phase type and a limited amount of yttria-alumina oxides residing mainly at the multi-grain junctions [86,87]. The CTE of the NLS SiC is entirely consistent with that for high-purity CVD SiC, explaining the complete lack of microcracks within or near the bonding layer in the TEPs/CVD. The lack of process-induced cracking or debond resulted in the high strength of this joint, represented by the failure in the base material in all torsion tests. Pores observed in the bonding layer in Fig. 6(A and B), likely resulting from an uneven application of the slurry during specimen preparation, did not negatively affect the strength to an unacceptable extent.

As is common in the NITE-like SiC sintered at relatively low temperatures [88], the bonding layer consisted of areas with lesser and greater amounts of the yttria–alumina oxide residue, shown in darker and brighter contrasts, respectively, in Fig. 6. Interestingly, a thin oxide layer (typically ~1 μm-thick) was often present near the mid-plane of the bonding layer. Where this oxide layer is present, oxide in the other areas of the bonding layer tended to have segregated toward the oxide layer. It is speculated that the segregation of oxide particles toward the surface had occurred within the painted mixed (SiC and oxide) slurry to form an oxide scale at the surface during preparation of the joints, resulting in the observed inhomogeneity of microstructure. The fact that the presence of this oxide layer did not severely limit the joint strength suggests that the yttria–alumina oxide alone may be used to produce SiC joints of reasonable strength.

As discussed previously, the remarkable increase in shear strength of the TEPs/CVD specimens from ~150 MPa for unirradiated condition to ~250 MPa after irradiation is considered an artifact. However, a slight increase in shear strength after irradiation may be true because the post-irradiation shear strength measured appeared consistently higher than the highest strength of the unirradiated joints. Irradiation-induced toughening of CVD SiC has been reported under similar irradiation conditions [77,78]. The effects of irradiation were not found in microstructures of the bonding layer, the oxide band, or the transition zone to the base material.

4.2.3. TEP tape-joined CVD SiC and NITE-like SiC

Backscattered scanning electron images of the cross-sectional samples of the TEP tape-bonded CVD SiC and NITE-like SiC are shown in Fig. 7. The SiC substrates of both types appeared to be seamlessly bonded as the TEP process sintered the substrate together with the SiC-based bonding agent, in the same way as the slurry-based TEP method. Because of the lack of distinct interfaces with the substrates, the bonding layer thickness could only be roughly estimated to be ~60 μm, assuming that the band containing the scattered residue of the oxide sintering additives in the TEPt/CVD joint corresponded with the bonding layer.

Outstanding microstructural features in the tape-based TEP joint are apparent in Fig. 7 when compared with the slurry-based one. First, the bonding layer appears to be sintered to a substantially greater extent than the slurry-based bonding layer, as characterized by the larger SiC crystal grains and the larger and more distinctive oxide domains, in spite of the lower sintering temperature and pressure (1850 °C and 10 MPa as compared with 1900 °C and 20 MPa for the slurry process). Second, substantial porosity due to pore sizes ranging mostly from sub-micron to ~10 μm is present along the mid-plane in the bonding layer, likely due to gas evolution from the organic binder that is used to prepare the tape. Third, the oxide residue appears to have segregated toward the porous mid-plane. These microstructural features imply that the sintering process did not take place homogeneously but started from the original surfaces of the SiC substrates then propagated toward the mid-plane as the sintering additives and the confined gas segregated with the propagating consolidation front. Another possible explanation is potential compositional inhomogeneity within the green tape across its thickness.

The tape-derived TEP joining demonstrated a high shear strength of >~150 MPa in the as-joined condition. Compared with the hand-painted slurry-derived joints for the identical substrate, the green tape joining seems to offer a significantly less specimen-to-specimen variation in strength. The lower strength compared with the slurry-derived joints (high-strength populations for the case of CVD SiC substrate) is likely resulting from the porous bonding layer. Under that assumption, the crack has to initiate from the porous bonding layer; thus, it is the seamless joint structure in addition to the decent strength of the bonding layer itself that made the apparent failure in the base material. No effects of neutron irradiation on shear strength and the SEM microstructures are evident.

4.2.4. TEP slurry-joined NITE SiC/SiC

The TEP slurry process produced an intact and robust joint of NITE SiC/SiC composite, as shown in Fig. 8 and as discussed earlier. The bonding layer appeared to be 50–60 μm thick, consistent with the joints of monolithic SiC processed under identical conditions. Interestingly, the oxide residue in this joint segregated toward

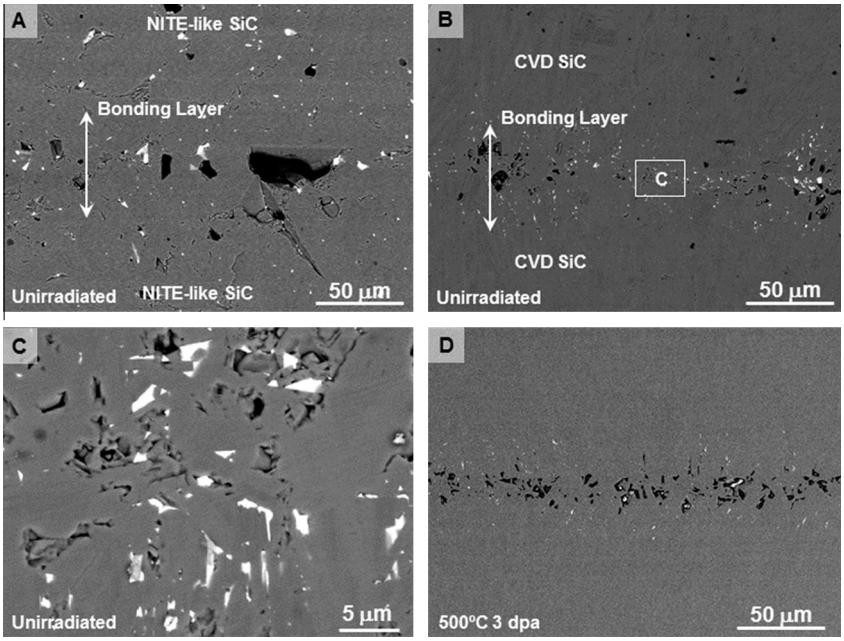

Fig. 7. Cross-sectional backscattered electron image of TEP (tape)–bonded NITE-like SiC (A) and CVD SiC (B–D) in as-joined (A–C) and neutron-irradiated (D, 3 dpa at 500 °C) conditions. Micrograph C was taken approximately at the location shown by the rectangle in micrograph B.

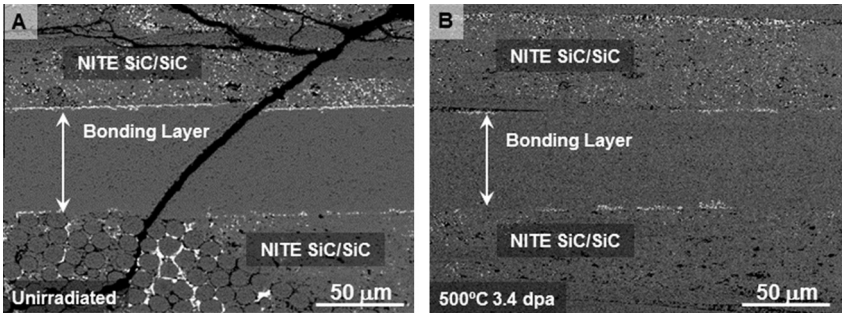

Fig. 8. Cross-sectional backscattered electron image of TEP slurry-joined NITE SiC/SiC composite before (A) and after (B) irradiation to 3 dpa at 500 °C. The pre-irradiation micrograph of a specimen was taken after a torsional shear test.

the interfaces with the composite substrates, unlike in the monolithic joints where distinctive oxide bands were observed near the mid-plane of the bonding layer. However, because these composite joint samples exhibited a high shear strength approaching 200 MPa, the presence of these oxide-rich interfaces on the mechanical properties is considered insignificant. Irradiation effects on microstructures or strength were not obvious.

A close look at Fig. 8 reveals a slight deformation of the Tyranno™ SA3 fibers, with their originally round cross sections transforming into slightly polygonal shapes. This is explained by the rather harsh joining process conditions involving an uni-axial pressure of 20 MPa and a temperature of 1900 °C, which somewhat exceed both the fiber and the composite processing temperatures. Therefore, the potential detrimental effects of this joining method on the composite properties will have to be addressed before it is used to join the composite materials.

The micrograph in Fig. 8(A) is a fragment of a torsion-tested specimen near its circumference. The fragment did not undergo further disintegration despite the extensive cracking shown, whereas most monolithic materials' joints shattered into smaller pieces upon fracture in the base material, demonstrating the damage tolerance of the composite joint. Since the main crack in Fig. 8(A) was propagating from the top right corner of the micrograph in a downward left direction, as evidenced by the crack branching morphology, this particular crack had initiated within the base composite on the top. It is also noted that the crack runs at an angle of approximately 45°, or perpendicular to the tensile stress component in the shear-loaded specimen.

4.2.5. CA glass–ceramic-joined CVD SiC

The microstructures of the CA glass–ceramic-joined SiC in the as-heat-treated condition are shown in Fig. 9(A and B). As well documented elsewhere [16,74], the CA bonding layer appears to consist of two distinctive phases in the backscattered electron images. The dominant, equiaxed island-like phase with the brighter contrast in backscattered electron images is reportedly a mixture of $3CaO{\cdot}Al_2O_3$and $12CaO{\cdot}7Al_2O_3$ [74]. The background matrix phase with the darker contrast also consists of multiple phases that are mostly crystalline ceramics and possibly a slight amount of amorphous phase, still to be quantified. Detailed transmission electron microscopy analysis is currently being conducted and will be published in a separate communication [89].

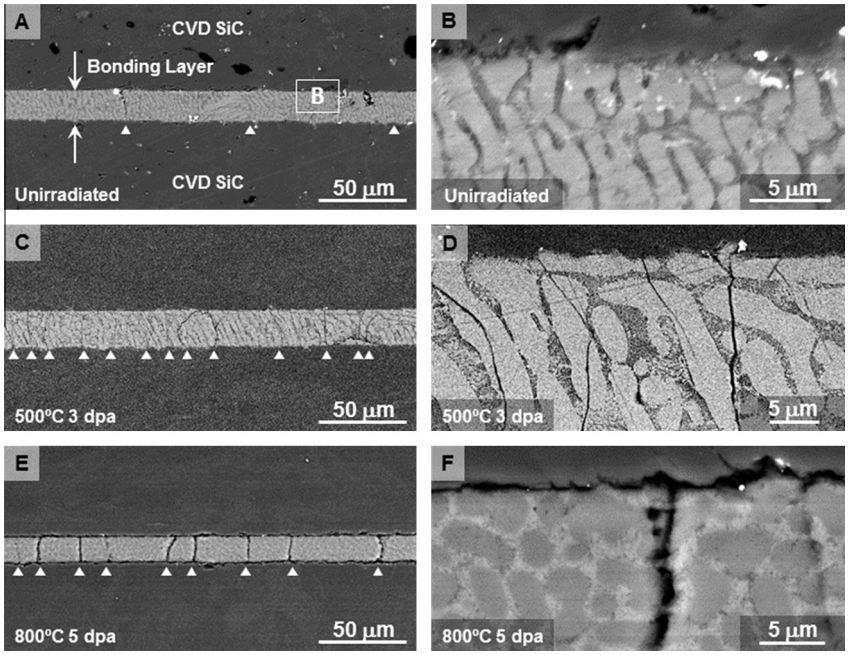

Fig. 9. Cross-sectional backscattered electron images of calcia–alumina glass–ceramic-joined CVD-SiC in unirradiated (A and B) and irradiated (C and D, 3 dpa at 500 °C; E and F, 5 dpa at 800 °C) conditions. Triangular symbols indicate transverse cracks in the bonding layer.

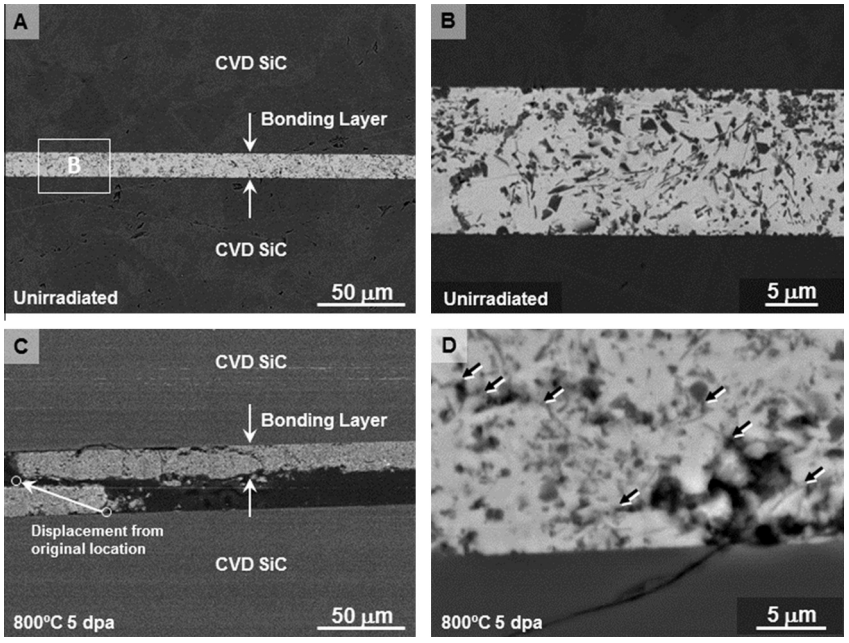

Fig. 10. Cross-sectional backscattered electron image of Ti–Si–C MAX phase-joined CVD-SiC in unirradiated (A and B) and irradiated (C and D, 5 dpa at 800 °C). Arrows in subset D indicate microcracks.

The as-heat-treated CA glass–ceramic layer exhibited transverse cracks running across the bonding layer, as shown in Fig. 9(A) by the triangular symbols, at an average interval of ~100 μm. These transverse cracks are typical of those introduced due to the CTE mismatch. However, no crack deflection along the interface with the CVD SiC substrate was observed, indicating reasonable interface toughness.

Following irradiation to 3 dpa at 500 °C, the transverse crack spacing obviously decreased to 10–20 μm, as shown in Fig. 9(C) and (D). Some of those cracks appear to be more open than the cracks observed in the unirradiated joints. The equiaxed appearance of the island phase in a lower atomic number matrix remained unaltered after irradiation. These observations seem to present an example of joint cracking resulting from the excess swelling of the substrates as compared to the bonding material. No interfacial debond was observed. The possible slight decrease in shear strength after neutron irradiation may thus be attributed to the increased transverse crack density.

Neutron irradiation at 800 °C to 5 dpa resulted in more substantial modifications in the observed microstructures. The low magnification SEM in Fig. 9(E) clearly presents transverse cracks that are open wider than in the unirradiated or 500 °C-irradiated joints,

while the transverse crack density appears lower than after 500 °C irradiation. The interface between the CA layer and the CVD SiC substrate appears to be at least partially debonded. Since swelling of SiC is less at a higher irradiation temperature, the more extensive crack opening at 800 °C than at 500 °C indicates a substantial irradiation effect on CA glass–ceramic.

The higher magnification backscatter electron (BSE) micrograph in Fig. 9(F) reveals more microstructural features that are specific to this high irradiation temperature. The elongated and equiaxed texture of the island phase has transformed into more roundish shapes. Moreover, the contrast in BSE images has switched between the island and the background matrix phases. The transverse cracks appeared to be bridged by the matrix phase, as shown in Fig. 9(F), implying a certain degree of plasticity of the matrix phase during irradiation at 800 °C. It is surprising to observe this major microstructural transition in the same joint that retained ~80% of the unirradiated shear strength after irradiation at 800 °C. More detailed examination is necessary to fully characterize the effects of irradiation on the mechanical properties and microstructures of this joint.

4.2.6. Ti–Si–C MAX phase-joined CVD SiC

Cross-sectional SEM images of the CVD SiC joined together by the Ti–Si–C MAX phase ceramic are presented in Fig. 10. Both unirradiated and irradiated microscopy specimens were prepared from the shear-tested broken specimens. The bonding layer was approximately 15 μm thick and consisted primarily of a continuum of Ti_3SiC_2 ternary ceramic that embeds SiC second phase in it (blocky or needle-like inclusions with dark contrast in Fig. 10(B)). The microstructures of this bonding material are well documented in Ref. [55] and reportedly involve small amount of TiC and $TiSi_2$. It is particularly noteworthy that no transverse cracks or finer microcracks were found in the bonding layer or at the interfaces during the SEM examination, despite the substantial mismatch between the SiC CTE and the orientation-averaged CTE for Ti_3SiC_2, likely owing to the decent toughness of this ternary ceramic itself and the effect of compositing with SiC particles/needles. In fact, a separate work conducted at ORNL indicates that a near-single-phase Ti_3SiC_2 joint of SiC develops microcracks that do not extensively propagate across the bonding layer [52].

Since all the irradiated torsion specimens exhibited a flat failure at the joined plane, the microscopy specimen was prepared so that the two mating fracture surfaces face each other. Because of the imperfect matching of the two faces, there remained a gap that was approximately the same height as the bonding layer thickness, as shown in Fig. 10(C). The crack clearly propagated along the interface between the bonding layer and the substrate, indicating a mostly cohesive failure of the joint. However, the interface bonding appeared intact before the forced debond, as evidenced in Fig. 10(D) where a crack excursion into the CVD SiC substrate is shown. In the layer of Ti_3SiC_2, microcracks with frequent deflections were observed. It was not possible to determine whether or not these microcracks are located along the grain boundaries. Parts of the SiC grains that were dispersed in the Ti_3SiC_2 matrix appeared to have come loose when exposed at the polished surface after microcracking within the SiC grains, implying substantial residual stress and/or the matrix microcracks propagating across the phase boundaries. However, extensive propagation of those microcracks was not observed.

4.3. Summary discussion

As discussed above, the effects of neutron irradiation at these low to intermediate fluence levels on the microstructures of various SiC joints ranged from a complete lack of apparent microstructural modification at the SEM level (TEP joints) to fine microcracking (titanium diffusion and Ti_3SiC_2 MAX phase) and enhanced lateral cracking accompanied by apparent microstructural modification (CA glass–ceramic joint in certain irradiation conditions). As expected, the general advantage of SiC-based bonding material was very clearly demonstrated in terms of irradiation effects on both strength and microstructural stability.

Despite apparent microstructural modifications in some joints under certain conditions, irradiation of all the evaluated joints, as tested by torsion of hourglass specimens, had no significant effect on shear strength. This result indicates that the shear strength of these joints is generally not very sensitive to the increased transverse crack density and randomly oriented slight microcracking within the bonding layer, as long as the interfacial adhesion maintains integrity. Morphologically rough interfaces between the base materials and the bonding layer seem to further desensitize the joint shear strength to microstructural damages likely through a mechanical interlocking effect. While this result is encouraging, it also implies that more comprehensive evaluation may be appropriate to fully characterize the irradiation effects. For example, tensile strength evaluation in an orientation perpendicular to the joint face will be able to better detect the adhesive strength change, in particular when a mechanical interlocking of rough interface is involved. Moreover, for applications in which hermeticity is a requirement (such as the LWR fuel rod plugging), a direct permeability measurement with a pertinent gas or liquid medium will be required since the shear strength did not appear sensitive to the cracks running across the entire bonding layer.

The present study demonstrated that the differential irradiation strain between the base SiC material and the bonding material imposes issues related primarily to hermeticity. As discussed previously, SiC is known to undergo substantial swelling in which the saturation level is a function of temperature. No other material swells in exactly the same way as SiC. Most materials exhibit less swelling at relatively low fluence levels. Therefore, transverse cracking during irradiation is inevitable unless a SiC-based bonding material is used or the bonding material is capable of deforming as SiC swells (elastically, plastically, including irradiation creep, or pseudo plastically). Since the CTE of SiC is smaller than many other materials, the transverse cracks may already be developed during the joint processing, as demonstrated by the titanium diffusion bonding described in this study. The openings in these cracks naturally increase when SiC swells more than the bonding material does. The differential straining through these two mechanisms, which results in the transverse cracking in flat joints where the constraint is only two-dimensional, may cause a substantial transverse tensile stress in three-dimensional structures such as the tube end plugging, possibly leading to a debond failure. This represents an inherent limitation in evaluating irradiation effects using a test specimen involving only flat bond plane.

Finally, although the effects of neutron irradiation on SiC-based structures with several joining technologies were favorably addressed in the present study, substantial future investigation is required for specific end applications. In addition to the hermetic property requirement discussed previously, chemical compatibility needs to be thoroughly examined as the critical feasibility issue. Such issues include the oxidation behavior of the joints in a chemically controlled helium flow for gas-cooled nuclear systems, water dissolution susceptibility for the LWR clad application, and corrosion in air and steam in accident scenarios for certain reactor systems.

5. Conclusions

Various methods of joining were applied to prepare joints of SiC ceramics and composites for evaluation of torsional shear strength,

microstructures, and the effects of neutron irradiation at elevated temperatures. All methods applied produced strong joints with unirradiated torsional shear strengths ~100 MPa or higher. The main conclusions of this study are summarized below.

(1) Diffusion bonding with titanium active insert resulted in a CVD SiC joint of reasonable shear strength when a Ti_3SiC_2/Ti_5Si_3 layered microstructure is obtained. The effects of irradiation at 500 °C to ~3 dpa appeared insignificant.
(2) TEP joining using SiC–Al_2O_3–Y_2O_3-based slurry produced very robust joints of CVD SiC, NITE-like sintered SiC, and NITE SiC/SiC composite. Joining process-induced damage to the composite integrity was identified as a potential concern. The effects of irradiation at 500 °C to ~3 dpa appeared insignificant.
(3) TEP joining using a commercial SiC–Al_2O_3–Y_2O_3-based green tape produced robust joints of CVD SiC and NITE-like sintered SiC. The joint strength is likely limited by a porous microstructure within the joint plane. The effects of irradiation at 500 °C to ~3 dpa or at 800 °C to ~5 dpa appeared insignificant or minor.
(4) CaO–Al_2O_3 glass–ceramic-joined CVD SiC exhibited reasonable shear strength. The effects of neutron irradiation on shear strength appeared minor or insignificant. Microstructural features remain unaltered after irradiation at 500 °C to ~3 dpa, whereas the irradiation at 800 °C induced observable microstructural evolution.
(5) Ti_3SiC_2-based joint of CVD SiC exhibited reasonable shear strength. The effects of neutron irradiation at 800 °C to ~5 dpa on shear strength and microstructures appeared minor or insignificant. Microcracks were present in the irradiated Ti_3SiC_2 layer.

The irradiation effects on the bonding material itself and the differential strain between the bonding material and the SiC base material were identified to have caused the observed irradiation effects in the joints. General advantages of the SiC-based bonding materials were confirmed. The need for additional studies, including a non-shear mechanical test, a permeability test, and irradiation in an application-relevant constraining condition, was identified for a full evaluation of the effects of irradiation on SiC-based structures used in joining technologies.

Acknowledgments

This work was supported by Office of Fusion Energy Sciences, US Department of Energy under contract DE-AC05-00OR22725 with UT-Battelle, LLC, and US-Japan TITAN Collaboration on Fusion Blanket Technology and Materials. Research supported in part by ORNL's Shared Research Equipment (ShaRE) User Facility and High Flux Isotope Reactor, which are sponsored by the Office of Basic Energy Sciences, U.S. Department of Energy. The authors are thankful to K.A. Terrani for providing a technical review of the manuscript and useful discussion, K. Toyoshima for microscopy, R.A. Meisner for XRD analysis, and S.M. Curlin, P.S. Tedder, and A.M. Williams for support in post-irradiation examination.

This manuscript has been authored by the Oak Ridge National Laboratory, managed by UT-Battelle LLC under Contract No. DE-AC05-00OR22725 with the US Department of Energy. The US Government retains and the publisher, by accepting the article for publication, acknowledges that the US Government retains a nonexclusive, paid-up, irrevocable, worldwide license to publish or reproduce the published form of this manuscript, or allow others to do so, for US Government purposes.

References

[1] R.H. Jones, C.H. Henager Jr., G.W. Hollenberg, J. Nucl. Mater. 191–194 (1992) 75–83.
[2] L.L. Snead, R.H. Jones, A. Kohyama, P. Fenici, J. Nucl. Mater. 233–237 (1996) 26–36.
[3] L. Giancarli, H. Golfier, S. Nishio, A.R. Raffray, C.P.C. Wong, R. Yamada, Fusion Eng. Des. 61–62 (2002) 307–318.
[4] A.R. Raffray, L. El-Guevaly, S. Gordeev, S. Malang, E. Mogahed, F. Najmabadi, I. Sviatoslavsky, D.-K. Sze, M.S. Tillack, X. Wang, A. Team, Fusion Eng. Des. 58–59 (2001) 549–553.
[5] L.A. El-Guebaly, A. Jaber, S. Malang, A.-A. Team, Fusion Sci. Tech. 61 (2012) 321–331.
[6] S. Nishio, S. Ueda, I. Aoki, R. Kurihara, T. Kuroda, H. Miura, T. Kunugi, Y. Seki, T. Nagashima, M. Ohta, J. Adachi, S. Yamazaki, I. Kawaguchi, T. Hashimoto, K. Shinya, Y. Murakami, H. Takase, T. Nakamura, Fusion Eng. Des. 41 (1998) 357–364.
[7] Y. Katoh, L.L. Snead, T.D. Burchell, W.E. Windes, Composite materials for high temperature reactors: technology development roadmap, in: 5th International Conference on High Temperature Reactor Technology, Prague, 2010.
[8] S. Sharafat, A. Aoyama, N. Morley, S. Smolentsev, Y. Katoh, B. Williams, N. Ghoniem, Fusion Sci. Tech. 56 (2009) 883–891.
[9] M. Ferraris, M. Slavo, V. Casalegno, A. Ciampichetti, F. Smeacetto, M. Zucchetti, J. Nucl. Mater. 375 (2008) 410–415.
[10] M. Ferraris, M. Salvo, V. Casalegno, S. Han, Y. Katoh, H.C. Jung, T. Hinoki, A. Kohyama, J. Nucl. Mater. 417 (2011) 379–382.
[11] B.V. Cockeram, J. Am. Ceram. Soc. 88 (2005) 1892–1899.
[12] T. Hinoki, N. Eiza, S.J. Son, K. Shimoda, J.K. Lee, A. Kohyama, Ceram. Eng. Sci. Proc. 26 (2005) 399–405.
[13] W. Lippmann, J. Knorr, R. Wolf, R. Rasper, H. Exner, A.M. Reinecke, M. Nieher, R. Schreiber, Nucl. Eng. Des. 231 (2004) 151–161.
[14] Y. Katoh, A. Kohyama, T. Nozawa, M. Sato, J. Nucl. Mater. 329 (2004) 587–591.
[15] H.C. Jung, Y.H. Park, J.S. Park, T. Hinoki, A. Kohyama, J. Nucl. Mater. 386–388 (2009) 847–851.
[16] Y. Katoh, M. Kotani, A. Kohyama, M. Montorsi, M. Salvo, M. Ferraris, J. Nucl. Mater. 283 (2000) 1262–1266.
[17] B. Riccardi, C.A. Mannetti, T. Petrisor, J. Woltersdorf, E. Pippel, S. Libera, L. Pilloni, J. Nucl. Mater. 329–333 (2004) 562–566.
[18] M. Singh, J. Mater. Sci. Lett. 17 (1998) 459–461.
[19] A. Gasse, F. Saint Antonin, G. Coing Boyat, Specific nonreactive brasic alloys for SiC–SiC joining, CEA-Grenoble, DEM n.DR 25: 97, in: Commissariat à l'énergie atomique et aux énergies alternatives, Grenoble, France, 1997.
[20] A.R. Raffray, R. Jones, G. Aiello, M. Billone, L. Giancarli, H. Golfier, A. Hasegawa, Y. Katoh, A. Kohyama, S. Nishio, B. Riccardi, M.S. Tillack, Fusion Eng. Des. 55 (2001) 55–95.
[21] C.A. Lewinsohn, R.H. Jones, M. Singh, T. Nozawa, M. Kotani, Y. Katoh, A. Kohyama, Ceram. Eng. Sci. Proc. 22 (2001) 621–626.
[22] M. Singh, Key Eng. Mater. 415 (1999) 164–165.
[23] B.H. Rabin, G.A. Moore, Mater. Res. Soc. Symp. Proc. 314 (1993) 197–203.
[24] C.H. Henager Jr., Y. Shin, Y. Blum, L.A. Giannuzzi, B.W. Kempshall, S.M. Schwarz, J. Nucl. Mater. 367–370 (2007) 1139–1143.
[25] C.H. Henager Jr., Y. Shin, R.H. Jones, Y. Blum, L.A. Giannuzzi, S.M. Schwarz, Coating and joining for SiC/SiC composites using preceramic polymers, in: A. Kohyama, R.H. Jones, B. Riccardi (Eds.), The Sixth IEA International Workshop on SiC/SiC Ceramic Composites for Fusion Applications, Boston, Massachusetts, USA, 2004, pp. 46–62.
[26] S. Yajima, K. Okamura, T. Shishido, Y. Hasegawa, T. Matsuzawa, Am. Ceram. Soc. Bull. 60 (1981) 253.
[27] W.J. Sherwood, C.K. Whitmarsh, J.M. Jacobs, L.V. Interrante, Ceram. Eng. Sci. Proc. 18 (1997) 177–184.
[28] S. Harrison, H.L. Marcus, Mater. Des. 20 (1999) 147–152.
[29] M.C. Halbig, M. Singh, T.P. Shpargel, J.D. Kiser, Ceram. Eng. Sci. Proc. 27 (2006) 133–143.
[30] B. Gottselig, E. Gyarmati, A. Naoumidis, H. Nickel, J. Eu. Ceram. Soc. 6 (1990) 153–160.
[31] B.V. Cockeram, The diffusion bonding of silicon carbide and boron carbide using refractory metals, in: Bettis Atomic Power Laboratory, West Mifflin, Pennsylvania, 1999.
[32] M. Omori, H. Takei, J. Am. Ceram. Soc. 65 (1982) C-92.
[33] S.M. Dong, Y. Katoh, A. Kohyama, J. Am. Ceram. Soc. 86 (2003) 26–32.
[34] Y. Katoh, S.M. Dong, A. Kohyama, Fusion Eng. Des. 61–2 (2002) 723–731.
[35] T. Koyanagi, K. Ozawa, T. Hinoki, K. Shimoda, Y. Katoh. Effects of neutron irradiation on mechanical properties of silicon carbide composites fabricated by nano-infiltration and transient eutectic-phase process, J. Nucl. Mater., 448 (2014) 478–486, http://dx.doi.org/10.1016/j.jnucmat.2013.10.005..
[36] M. Ferraris, V. Casalegno, S. Rizzo, M. Salvo, T.O. Van Staveren, J. Matejicek, J. Nucl. Mater. 429 (2012) 166–172.
[37] M. Ferraris, M. Salvo, S. Rizzo, V. Casalegno, S. Han, A. Ventrella, T. Hinoki, Y. Katoh, Int. J. Appl. Ceram. Technol. 9 (2012) 786–794.
[38] D.L. Porter, M.R. Pascucci, B.H. Olbert, J. Nucl. Mater. 103 (1981) 767–771.
[39] W.A. Coghlan, F.W. Clinard Jr., J. Nucl. Mater. 179–181 (1991) 391–394.
[40] F. Mailliart, V. Hodaj, N. Eustathopoulos, Mater. Sci. Eng. A 495 (2008) 174–180.
[41] G. Chaumat, B. Drevet, L. Vemier, J. Eu. Ceram. Soc. 17 (1997) 1925–1927.
[42] G. Chaumat, P. Le Gallo, G. Le Marois, F. Moret, P. Deschamp, J. Nucl. Mater. 233–237 (1996) 932–934.

[43] F. Moret, P. Sire, A. Gasse, Brazing of SiC and SiC based materials using the BraSiC process chemical and thermal applications, in: International Conference on Joining of Advanced Materials, Rosemont, 1998.
[44] J.C. Corelli, J. Hoole, J. Lazzaro, C.W. Lee, J. Am. Ceram. Soc. 66 (1983) 529–537.
[45] R.B. Matthews, J. Nucl. Mater. 51 (1974) 203–208.
[46] R.A. Matheny, J.C. Corelli, J. Nucl. Mater. 83 (1979) 313–321.
[47] E.D. Herderick, K. Cooper, N. Ames, Adv. Mater. Proc. 170 (2012) 24–27.
[48] S. Suyama, Y. Itoh, A. Kohyama, Y. Katoh, J. Ceram. Soc. Japan 109 (2001) 315–321.
[49] Y. Katoh, H. Kishimoto, A. Kohyama, J. Nucl. Mater. 307 (2002) 1221–1226.
[50] E. Lell, N.J. Kreidl, J.R. Hensler, Radiation effects in quartz, silica and glasses, in: J.E. Burke (Ed.), Progress in Ceramic Science, Pergamon Press, 1966, pp. 1–87.
[51] M. Barsoum, T. El-Raghy, Am. Sci. 89 (2001) 334–337.
[52] T. Cheng, J.O. Kiggans, Y. Katoh, L.L. Snead, Process development and optimization for silicon carbide joining and irradiation studies, Fusion Materials, DOE/ER-0313/53, 2013, 42-54.
[53] H. Dong, W. Han, S. Li, Mater. Sci. Forum 475–479 (2005) 1255–1258.
[54] R. Radhakrishnan, C.H. Henager, J.L. Brimhall, S.B. Bhaduri, Script. Mater. 34 (1996) 1809–1814.
[55] C.H. Henagar Jr., R.J. Kurtz, J. Nucl. Mater. 417 (2011) 375–378.
[56] G.W. Hollenberg, C.H. Henager Jr., G.E. Youngblood, D.J. Trimble, S.A. Simonson, G.A. Newsome, E. Lewis, J. Nucl. Mater. 219 (1995) 70–86.
[57] P. Colombo, B. Riccardi, A. Donato, G. Scarinci, J. Nucl. Mater. 278 (2000) 127–135.
[58] J.C. Nappé, I. Monnet, P. Grosseau, F. Audubert, B. Guilhot, M. Beauvy, M. Benabdesselam, L. Thomé, J. Nucl. Mater. 409 (2011) 53–61.
[59] L. Zhang, Q. Qi, L.Q. Shi, D.J. O'Connor, B.V. King, E.H. Kisi, D.K. Venkatachalam, Appl. Surface Sci. 258 (2012) 6281–6287.
[60] C.A. Lewinsohn, P. Colombo, I. Reimanis, O. Unal, J. Am. Ceram. Soc. 84 (2001) 2240–2244.
[61] C.A. Lewinsohn, R.H. Jones, P. Colombo, B. Riccardi, J. Nucl. Mater. 307–311 (2002) 1232–1236.
[62] H.-J. Kleebe, Y.D. Blum, J. Eu. Ceram. Soc. 28 (2008) 1037–1042.
[63] Y.D. Blum, D.B. MacQueen, H.-J. Kleebe, J. Eu. Ceram. Soc. 25 (2005) 143–149.
[64] S. Modena, G.D. Soraru, Y. Blum, R. Raj, J. Am. Ceram. Soc. 88 (2005) 339–345.
[65] L.L. Snead, M.C. Osborne, K.L. More, J. Mater. Res. 10 (1995) 736–747.
[66] L.V. Interrante, C.W. Whitmarsh, W. Sherwood, H.-J. We, R.S. Lewis, G. Maciel, Mater. Res. Soc. Symp. – Proc. 346 (1994) 593–603.
[67] M. Kotani, T. Inoue, A. Kohyama, Y. Katoh, K. Okamura, Mater. Sci. Eng. A – Struct. Mater. Prop. Microstruct. Process. 357 (2003) 376–385.
[68] Y. Katoh, M. Kotani, H. Kishimoto, W. Yang, A. Kohyama, J. Nucl. Mater. 289 (2001) 42–47.
[69] M.C. Halbig, M. Singh, H. Tsuda, Int. J. Appl. Ceram. Technol. 9 (2012) 677–687.
[70] L.M. Nguyen, O. Gillia, E. Riviere, D. Leguillon, Ceram. Eng. Sci. Proc. 31 (2010) 107–118.
[71] M. Singh, E. Lara-Curzio, J. Eng. Gas Turbines Power 123 (2001) 288–292.
[72] B. Riccardi, M. Sacchetti, C.A. Nannetti, J. Woltersdorf, E. Pippel, T. Petrisor, Progress in low activation brazing for SiCf/SiC ceramic matrix composites, in: R.H. Jones, B. Riccardi, A. Kohyama (Eds.), Fifth International Energy Agency Workshop on SiC/SiC Ceramic Composites for Fusion Energy Application, San Diego, California, 2002, pp. 65–68.
[73] A. Donato, P. Colombo, M.O. Abadirashid, Ceram. Trans. 57 (1995) 431–436.
[74] M. Ferraris, M. Salvo, C. Isola, M. Appendino Montorsi, A. Kohyama, J. Nucl. Mater. 258–263 (1998) 1546–1550.
[75] M. Ferraris, M. Salvo, V. Casalegno, A. Ventrella, M. Avalle, Int. J. Appl. Ceram. Technol. 9 (2012) 795–807.
[76] H.C. Jung, T. Hinoki, Y. Katoh, A. Kohyama, J. Nucl. Mater. 417 (2011) 383–386.
[77] L.L. Snead, T. Nozawa, Y. Katoh, T.S. Byun, S. Kondo, D.A. Petti, J. Nucl. Mater. 371 (2007) 329–377.
[78] Y. Katoh, L.L. Snead, J. ASTM. Int. 2 (2005). 12377-12371-12313.
[79] J.J. Williams, M.J. Kramer, M. Akinc, J. Mater. Res. 15 (2000) 1780–1785.
[80] S.B. Li, J.X. Xie, L.T. Zhang, L.F. Cheng, Mater. Sci. Technol. 21 (2005) 1054–1058.
[81] C. Kinoshita, S.J. Zinkle, J. Nucl. Mater. 233–237 (1996) 100–110.
[82] T. Yano, M. Akiyoshi, K. Ichikawa, Y. Tachi, T. Iseki, J. Nucl. Mater. 289 (2001) 102–109.
[83] T. Yano, K. Ichikawa, M. Akiyoshi, Y. Tachi, J. Nucl. Mater. 283–287 (2000) 947–951.
[84] L.L. Snead, Y. Katoh, S. Kondo, J. Nucl. Mater. 399 (2010) 200–207.
[85] T. Yano, K. Inokuchi, M. Shikama, J. Ukai, S. Onose, T. Maruyama, J. Nucl. Mater. 329–333 (2004) 1471–1475.
[86] T. Koyanagi, S. Kondo, T. Hinoki, Ceram. Eng. Sci. Proc. 32 (2011) 53–62.
[87] K.A. Terrani, J.O. Kiggans, Y. Katoh, K. Shimoda, F.C. Montgomery, B.L. Armstrong, C.M. Parish, T. Hinoki, J.D. Hunn, L.L. Snead, J. Nucl. Mater. 426 (2012) 268–276.
[88] S.M. Dong, Y. Katoh, A. Kohyama, J. Eu. Ceram. Soc. 23 (2003) 1223–1231.
[89] M. Ferraris, M. Salvo, V. Caselegno, S. Rizzo, A. Czyrska-Filemonowicz, T. Moskalewicz and Y. Katoh, Microstructure and properties of a CaO-Al_2O_3 glass-ceramic for pressure-less joining of SiC based components, J. Eu. Ceram. Soc., submitted for publication.